6 Influence of flaws and crystal properties on particle fracture in a jet mill

Abstract

Jet milling is commonly used for reducing the particle size of active pharmaceutical ingredients. Unfortunately, this process is sometimes difficult to control as pre-existing flaws and mechanical material properties affect the particle fracture behaviour in a mill. In this study the effect of pre-existing flaws on mechanical material properties of crystals of a model material, sodium chloride, from different sources have been investigated using optical microscopy, nanoindentation, and powder compaction. Subsequently, these properties have been correlated with particle fracture in a jet mill. This chapter shows that particles that have a small average flaw size possess the lowest constraint factor whereas particles that have a large average flaw size have a high constraint factor and hence behave more ductile. The constraint factor is defined as the ratio of the hardness and the yield pressure and is a measure for the ductility of the material. Moreover, the study shows that the rank orders of the mechanical material properties are consistent with the rank order of the experimentally determined particle rate of breakage. Materials that have a relatively low hardness show the highest particle rate of breakage. The degree of particle fracture during jet-milling tends to decrease for particles that have a smaller flaw density and behave more ductile. The paper shows that pre-existing flaws have an impact on mechanical material properties and on particle fracture behaviour in a jet mill. It is concluded that crystal's average flaw size and density of flaws has an impact on the mechanical material properties and hence, on the fracture behaviour of particles in a jet mill.

Powder Technology, 2007 (submitted)

6.1 Introduction

In recent years and particularly in the pharmaceutical industry, product quality criteria have become more and more strict, leading to specifications like a narrower particle size distribution and hence closer control of particle size. Active pharmaceutical ingredients (APIs) used in pharmaceutical product development are rarely ready for use as crystallised drug substance. Frequently, the particle size needs to be reduced in order to meet the specific requirements. For example, the route of administration dictates the particle size distribution, like pulmonal delivery for which typically particle sizes in the range of 1-6 micron are required (1). Jet milling is commonly used for reducing the particle size. Unfortunately, size reduction by milling has remained essentially an empirical science (2). It is not for lack of either interest or investigation that a quantitative theory of milling does not exist. The number of references in the literature dealing with milling is overwhelming mainly as an effect of the needs to maximise production capacity and to minimise energy consumption in the mineral industry. However, data of milling of pharmaceutical active materials are relatively scarcely published (3). Milling operations in pharmaceutical industry are generally limited to two or three types of equipment where the main criteria of choice is the ability to obtain a certain product quality, in terms of particle size or specific surface area. Despite intensive use and research the detailed mechanism of jet milling is not yet entirely understood (4). This leads to the situation that the milling conditions have to be determined for each material using pilot-scale trials. This is both material and time consuming (5). It is believed that both particle deformation and fracture mechanisms play an important role in particle breakage and hence in milling performance. The particle fracture behaviour of a material in general depends on the mechanical material properties of the material to be milled, processing conditions like stressing intensity, impact velocity, and the pre-existing imperfections and flaws in the material (6). The strength of different particles of identical material and identical size differ

because different flaws are present on the particle surface. Zügner et al (3) reported that elastic plastic properties of the materials to be milled are important as these determine the resistance against particle fracture as well as the formation and propagation of cracks. In the theory of milling it is common practice to evaluate the particle fracture behaviour as an entangled effect of pre-existing flaws and cracks as well as mechanical material parameters. Moreover, sometimes it is assumed that particle fracture behaviour is governed largely by pre-existing flaws. Currently, to the knowledge of the authors it is not clear whether either pre-existing flaws or mechanical material properties dominate particle fracture. The purpose of this study is to investigate the effect of pre-existing flaws and mechanical material parameters on particle fracture in a jet mill in order to improve control of the milling process.

6.2 Material and methods

6.2.1 Material

Sodium chloride has been chosen as a model compound. The reason for this choice is that different sources and production methods give different inclusions in the form of vacuoles (that contain brine) and other lattice defects, which offers the possibility of controlled variation of defects in the material. At the same time, the particle size and shape remain largely unchanged. Therefore, sodium chloride is a suitable model compound for this study. Sodium chloride crystals are cubic in shape and were produced by evaporation of pickling brine saturated in natural rock salt. All materials used were produced by Akzo Nobel at different production areas: salt 1 from Stade (Germany), salt 2 from Hengelo (The Netherlands), an intermediate quality salt 3 Mariager (Denmark), and Salt 4 from Stade which is chemically the purest salt. Sodium chloride crystals are cubic in shape and were produced by evaporation of pickling brine saturated in natural rock salt.

6.2.2 Methods

6.2.2.1 Determination of yield strength

The yield pressure was determined as proposed by Heckel (7). The porosity-pressure relation of the compounds was investigated using a high speed compression simulator (ESH, Brierley Hill, UK). This compression simulator enables the assessment of compaction behaviour with single tablets. A powder sample of 500 mg was compressed into a cylindrical compact with a diameter of 13 mm. Compression load and compact volume with time were recorded. The

average punch speed was 3 mm/s. The compression profile was sinusoidal. Heckel (7) suggested to linearise the porosity (ε)-pressure (P) relation of powders:

$$-\ln(\varepsilon) = K \cdot P_c + A \tag{1}$$

The symbol A is a constant which is thought to be a measure of the relative density of the powder bed after particle rearrangement (8). The linear part of the curve has slope K and this slope is related to the yield strength (σ_c) by:

$$\sigma_c = \frac{1}{3.K} \tag{2}$$

The yield pressure of a material is approximately equal to 3 times the yield strength (9). Hence, the reciprocal of K can be regarded as numerically equal to the mean yield pressure:

$$P_y = 3 \cdot \sigma_c = \frac{1}{K} \tag{3}$$

6.2.2.2 Sample preparation for indentation

Reproducible nanoindentation measurements can be performed only on smooth and almost horizontal surfaces. The nano-indentation samples had to be processed in a special way, avoiding use of water which would dissolve the material. The crystals were embedded in epoxy (containing no water). Subsequently, the samples were dry-ground (i.e. using no lubricant) according to the DIN-norm using, consecutively silicon carbide abrasive paper with decreasing coarseness: Grit 800 (~0.5 mm), Grit 1200 (~0.1 mm), Grit 2400, and Grit 4000. After this, a polishing step of 75 seconds was carried out, using 0-1 μm diamond powder on a Dur-polishing cloth (Struers), using ethanol P.A. as a lubricant. As shown in Figure 6-1, the procedure resulted in very smooth crystal surfaces, with a typical roughness (Ra) smaller than 0.5 μm.

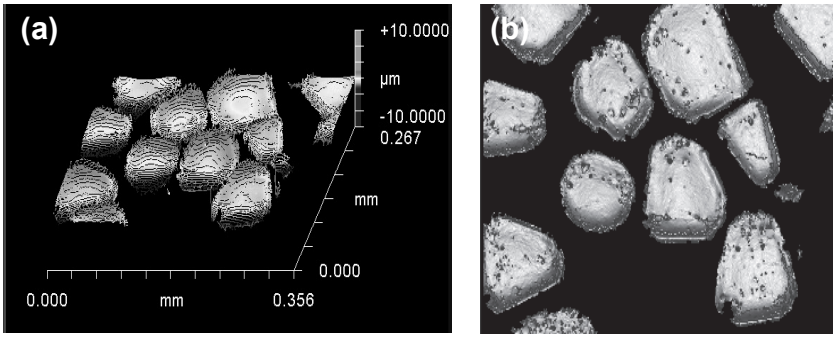

Figure 6-1 Micrographs of the polished crystals for nanoindentation; (a) Optical Interferometry plot (Zygo); (b) bright field optical micrograph.

6.2.2.3 Indentation procedure

In indentation, a sharp diamond pyramidal tip (an "indenter") is pressed into the surface of the material, while the force on the tip and the penetration depth of the indenter into the material is measured. From the resulting force-displacement curve, together with subsequent observation of the probed surface, the static mechanical properties can be determined. Load-control nanoindentation tests (Nano Indenter XP, MTS Systems Co., Oak Ridge, TN) were performed on the embedded specimens using a Berkovich diamond indenter. The tests were performed in a vibration isolation cabinet at room temperature and stable humidity to ensure that the influence from thermal drift was minimal. The loading rate was $(dP/dt)/P = 0.075\,\mathrm{s}^{-1}$, and the maximum indentation depth was 1 µm. After reaching the maximum depth, the force was kept constant for 10 s, after which the unloading took place at $(dP/dt)/P = 0.075\,\mathrm{s}^{-1}$.

From this protocol load-displacement curves were obtained and the Oliver and Pharr method (10) was applied to determine the elastic modulus and the hardness. Using the contact area A_c,

and the contact stiffness *S*, which is the slope of the initial portion of the final unloading curve, assumingly representing a purely elastic effect, the reduced modulus (E_r) of the specimen-indenter combination was determined according to:

$$E_r = \frac{\sqrt{\pi}}{2}\frac{S}{\sqrt{A_c}} \tag{4}$$

whereas the hardness (*E*) was estimated using:

$$H = \frac{P_{\max}}{A_c} \tag{5}$$

in which $P_{\max}$ is the load at maximum displacement (just before unloading). The contact area A_c was determined from the load-displacement curve according to the method described by Oliver and Pharr (10). For this method, the tip shape of the indenter needs to be known, and this was determined using calibration measurements on fused silica. The specimen (crystal) modulus (*E*) follows from:

$$E = \frac{1-\nu_c^2}{\frac{1}{E_r} - \frac{1-\nu_i^2}{E_i}} \tag{6}$$

where ν is the Poisson's ratio and the subscripts *c* and *i* refer to the crystal specimen and the indenter respectively, and E_i is the indenter's Young's modulus. The elastic properties of the Berkovich diamond indenter are: $\nu_i = 0.07$ and $E_i = 1140$ GPa. The Poison's ratio of the sodium chloride crystal was assumed to be 0.18.

6.2.2.4 Determination of flaws

To check for flaws, impurities and crystal defects the particles were investigated with an optical microscope (Jenaval, Zeiss, Jena, Germany). The method has been described in detail elsewhere (11). The detection of flaws in particles is limited to flaws larger than 1 micron.

6.3 Results and Discussion

6.3.1 Mechanical properties of starting materials

The static mechanical properties of crystals have been probed using nanoindentation. The yield pressure (P_y) of each type of salt has been determined by making a Heckel plot (7) as described in the materials and method section. Table 6-1 gives the values determined by nanoindentation and powder compaction. The table also contains two dimensionless numbers which will be discussed later.

Table 6-1 Mean mechanical material properties and constraint factor of sodium chloride particles of different sources.

Material	H (MPa)	E (GPa)	P_y (MPa)	H/P_y (-)	E/P_y (-)
Salt 1	308	39.9	86.8	3.5	459
Salt 2	262	30.8	100.7	2.6	306
Salt 3	266	30.9	105.6	2.5	293
Salt 4	319	40.5	87.2	3.6	465

It is noted that different sources of sodium chloride salts have different mechanical material properties which was not expected a priori. Table 6-1 shows that salts 1 and 4 can be assigned as salts having a relatively high hardness and high Young's modulus of elasticity, while, salts 2 and 3 are materials with a relatively low hardness and low Young's modulus of elasticity. Clearly, the mechanical material properties are different.

Basically, three types of material behaviour can be distinguished, i.e. elastic, elastic-plastic, and visco-elastic behaviour (12). Often the dimensionless ratios H/P_y and E/P_y are used to characterize materials (13). The ratio H/P_y is called the constraint factor (14) and is a measure for the ductility of the material. Very elastic materials have a H/P_y value of 1.5-2.0 (13).

Brittle materials have a H/P_y ratio of 2.0-2.2 (if $H/P_y > 2.2$ then there is tendency towards a reduction in brittle behaviour). Theoretically, a value of 3 is expected for perfectly rigid plastic and elastic-plastic materials (15). It is concluded that salts 2 and 3 have elastic mechanic material properties compared to salts 1 and 4 which have more ductile mechanical material properties.

The next step is to determine the flaw density of the sodium chloride particles. In this study the flaw density is defined as the total amount of flaws present per unit of area. Table 6-2 lists the flaw density and the average flaw size of the different types of sodium chloride particles. The average flaw size was taken from (11) and reproduced in tabular form. It is noted that the results in Table 6-2 are entangled: salts that are rich in flaws also contain small flaws, while the flaws in particles with a low flaw density are large.

Table 6-2 Flaw density and average flaw size of the different types of sodium chloride particles (particle size 300-425 μm) adapted from (11).

	Salt 1	Salt 2	Salt 3	Salt 4
Flaw density [flaws /m^2]	$6.05.10^9$	$13.8.10^9$	$8.98.10^9$	$6.81.10^9$
Average flaw size (μm)	7.3	5.3	5.7	6.8

The constraint factor (H/P_y) has been plotted as a function of the dimensionless ratio E/P_y of the four types of sodium chloride particles investigated (Figure 6-2). The numbers in Figure 6-2 represent the average flaw size.

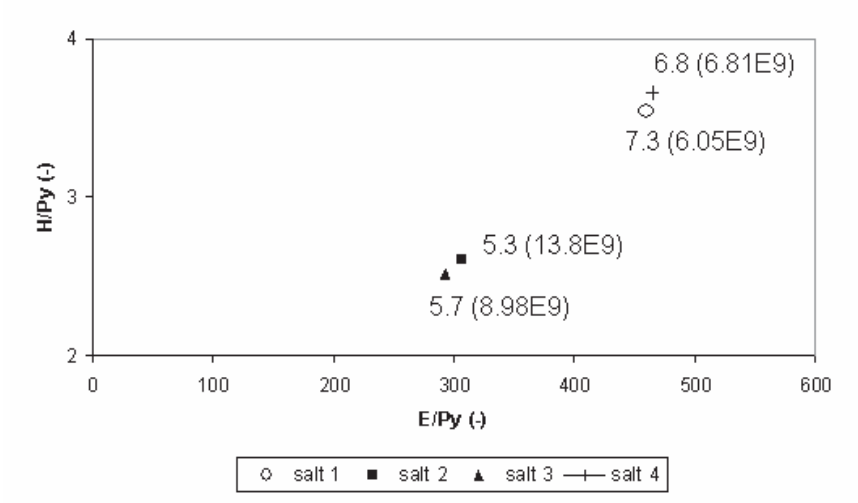

Figure 6-2 Relation between material properties of sodium chloride particles of different origin. The numbers represents the average flaw size in micrometer and the number between brackets represents the flaw density per unit of area.

The mechanical behaviour of the four different types of salts investigated can be classified in two distinct groups. It is observed that a correlation exists between the average flaw size (or flaw density but will not be indicated in the remainder of this section) and the mechanical material properties. Particles having a small average flaw size (i.e. salts 2 and 3) possess the lowest constraint factor while particles having a larger average flaw size (salts 1 and 4) have the largest constraint factor. This shows that materials having a large average flaw size behave more ductile. It is also concluded that the brittleness of all salts is low. This can be illustrated by the observation that the crystals behaved relatively tough during indentation measurements. No cracking occurred due to the indentation with the very sharp indenter up to loads of 20 N. For this reason, additional indentation experiments were performed using a cube corner with an included angle of 90° (the work done on the crystal is then greater at the same load, because the cone penetrates deeper into the crystal). Even in this situation no

cracks developed. Due to the fact that no cracks developed it was not possible to determine the fracture toughness of sodium chloride. This remarkable ductility has also been noted by other authors (16, 17) and appears to be consistent with the findings in this study.
The discussion so far relates to the characterization of four types of sodium chloride particles. The next step is to investigate the influence of the mechanical material properties and the flaw size on particle fracture behaviour during milling.

6.3.2 Milling experiments

In a fluidized bed opposed jet mill the particles to be ground are stressed by impact. As a result particles are reduced in size. The instrumentation of the mill allows adjustment and control of the operational parameters. If these parameters are kept constant, differences in particle size of the milled material are due to differences in properties of the feed material.
The milling behaviour can be quantified by the particle rate of breakage function, also called selection function or breakage probability (18, 19). The rate of breakage function (***S***) is the probability of a particle with a certain size to break per unit time. The particle rate of breakage functions of the four types of sodium chloride salts were adapted from (11) and reproduced in Figure 6-3 to allow re-analysis.

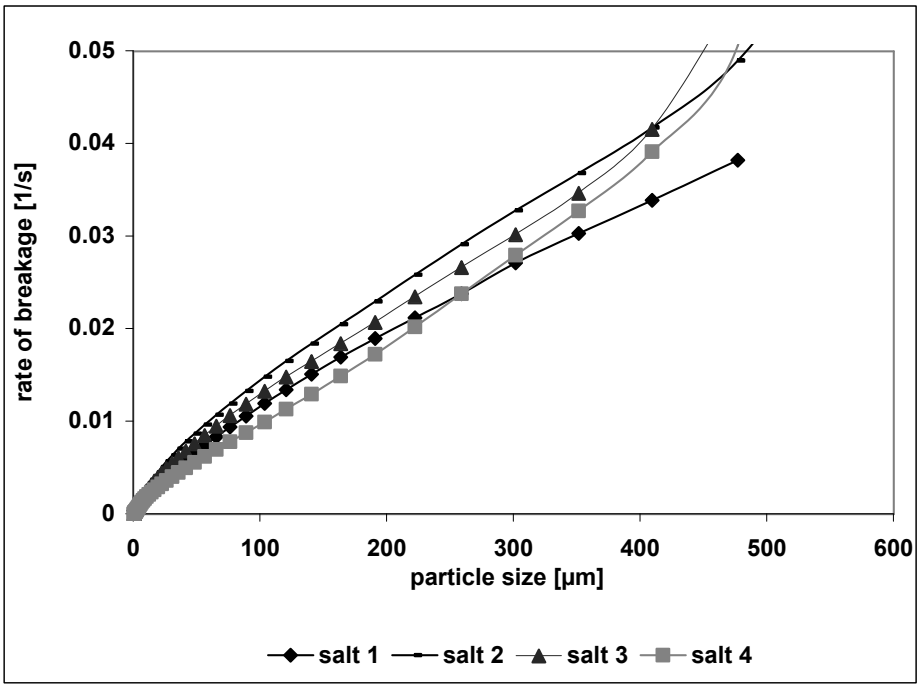

Figure 6-3 Particle rate of breakage of four types of salt of different type of origin. Milling pressure was 5 bar (11).

It is commonly accepted that due to the presence of flaws in particles, the particle strength increases with decreasing particle size (20). The low probability of finding a large flaw in a small particle explains the observed increase in the strength of smaller particles. Figure 6-3 shows that the particle rate of breakage is a function of particle size and this is consistent with theory (6, 20). Furthermore, each type of sodium chloride shows a distinct particle rate of fracture. This difference is not explained by the variation in the experimental set-up, since processing conditions were kept the same. Figure 6-4 shows the particle rate of breakage of the sodium chloride particles of different sources of size 350 micron as a function of their average flaw size. This figure illustrates that different types of materials show a distinct particle rate of fracture behaviour that correlates with the average flaw size. A similar but

inverse correlation can be found when the rate of breakage is plotted as a function of flaw density.

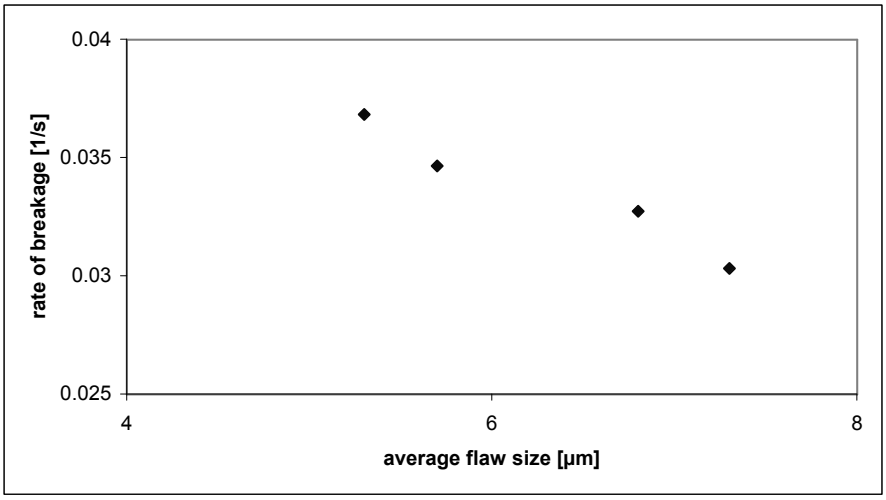

Figure 6-4 Particle rate of breakage of particles with a size of 350 micron versus the average flaw size of the different sources of sodium chloride particles.

Combining the particle rate of breakage data of Figure 6-3 with the mechanical material properties of Table 6-1 shows that materials with a relatively high average flaw size are more ductile during milling. Moreover, it is observed that sodium chloride particles (salts 2 and 3) that possess the lowest constraint factor and that have a relatively small average flaw size show the highest rate of breakage during milling. In contrast, sodium chloride particles (salts 1 and 4) with the highest constraint factor have a relatively large average flaw size and show the lowest rate of breakage during milling.

The discussion so far indicates that material properties and flaw size or flaw density determine particle breakage behaviour. It is unclear however, whether the impact of flaw size

is dominant or that of flaw density because the data are entangled. The next step is an attempt to separate these effects.

6.3.3 Particle strength of particles containing cracks and flaws

In this section the particle strength is calculated based on the interaction between flaws. Inglis (21) showed that flaws play a dominant role in particle fracture as the local stresses generated at the tips of the flaws are much higher than the loading stress. During stressing of particles wing cracks grow from these flaws near the tips of the initial flaw, where the tensile stress is a maximum, and then propagate at sharp angles from the pre-existing crack direction to become parallel to the direction of axial compression (22). These cracks propagate and start to interact with neighbouring cracks and this leads to crack coalescence and finally, macroscopic, particle fracture. Nemat-Nasser and Horri (23, 24) investigated the mechanism of crack interactions and they showed that flaw length is one of the parameters controlling the failure pattern of specimens.

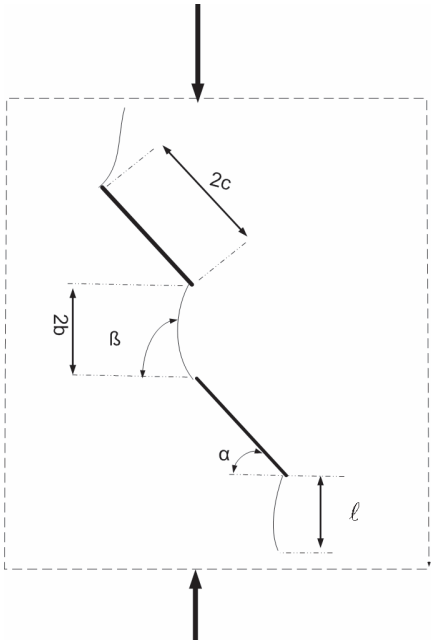

Figure 6-5 Wing crack propagation in a particle where 2*c* is the flaw length and 2*b* is the bridge distance between two flaws. (Adapted form Wong et al. (22)).

Figure 6-5 shows crack coalescence between two pre-existing flaws of length 2*c*. To calculate the particle strength of sodium chloride particles as a function of the number of flaws the model of Ashby-Halam (25) was employed. They derived an expression for the stress intensity factor K_{IC} at the tip of the wing cracks, which nucleates from a pre-existing inclined flaw of length *2c* when a particle is stressed (as illustrated in Fig. 6-5) and when crack interaction and crack coalescence occurs. Reworking their model results in:

$$\sigma = \frac{K_{IC}}{\sqrt{\pi\, c}} \left\{ \frac{(\sin 2\psi - \mu + \mu \cos 2\psi)}{(1+L)^{\frac{3}{2}}} \left[0.23\, L \frac{1}{\sqrt{3}\,(1+L)^{\frac{1}{2}}} \right] + \{2\varepsilon_o\, (L + \cos\psi)/\pi\}^{\frac{1}{2}} \right\}^{-1} \qquad (7)$$

where σ is the particle strength, K_{Ic} is the critical stress intensity that characterizes the crack resistance (0.5 MPa√m for sodium chloride (26), ψ is the angle measured from loading direction to the direction along the shear crack surface (i.e. ψ = 90° - α in which α is the flaw

angle, i.e. inclination of the flaw), $L = \ell / c$ the normalized length of the wing cracks (ℓ is the length of the wing crack as shown in Fig. 6-5 and $2c$ is the crack length of Table 6-3), μ the friction coefficient on the surface, and, finally, ε_o is the initial crack density ($\varepsilon_o = c^2 N$a, where Na is the number of flaws per unit area of Table 6-2). In this study it has been assumed that the friction coefficient μ is 0.6 which is a commonly used value (22-24).Table 6-3 lists the values used to calculate the particle strength σ of sodium chloride particles with a particle size of 350 µm.

Table 6-3 Values used to predicted the particle strength of sodium chloride particles (particle size 350 µm).

	K_{IC} (MPa√m)	μ (-)	Ψ (°)	L (-)	c (m)	Na (flaws/m^2)	εo (-)
Salt 1	0.5	0.6	45	2	$7.3.10^{-6}$	$6.05.10^{9}$	16.8
Salt 2	0.5	0.6	45	2	$5.3.10^{-6}$	$13.8.10^{9}$	38.1
Salt 3	0.5	0.6	45	2	$5.7.10^{-6}$	$8.98.10^{9}$	25.2
Salt 4	0.5	0.6	45	2	$6.8.10^{-6}$	$6.81.10^{9}$	18.9

Since it was not possible in this study to determine K_{Ic} experimentally, and since the stress intensity factor is a function of the flaw size (27) too, it is not possible to predict the precise particle strength of the four different sources of sodium chloride particles. However, keeping all parameters constant except the average flaw size (c) and the flaw density (N_a) it is possible to calculate the influence of these parameters individually on the particle strength. Figure 6-6 shows the influence of both the flaw density and the average flaw size on the predicted

particle strength of the four different sources of sodium chloride particles using eq. 7 and the values of Table 6-3.

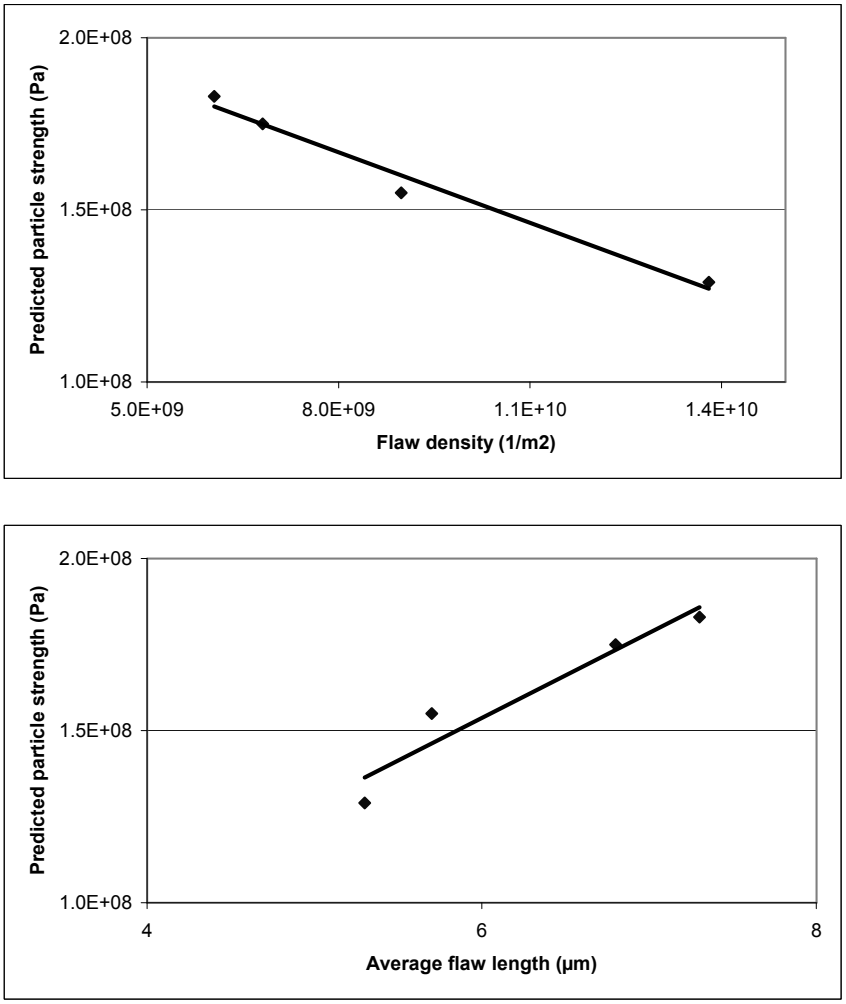

Figure 6-6 Predicted particle strength of sodium chloride particles as a function of flaw density and average flaw size (particle size 350 micron).

Figure 6-6 shows that both the flaw density and flaw size influences the particle strength but in a opposite manner. Since a difference in particle strength is observed between the same types of materials it is hypothesized that the reduction in particle strength is due to the increase of the number of flaws introduced in the crystal during milling rather than an increase in flaw length.

6.4 Conclusions

In this study the effect of pre-existing flaws on mechanical material properties of crystals of a model material, sodium chloride, from different sources have been investigated. These mechanical properties have been correlated with particle fracture in a jet mill.

This chapter shows that particles that have a small average flaw size or high flaw density possess a relatively small constraint factor whereas particles that have a high average flaw size have a high constraint factor and hence behave more ductile. On the basis of an existing model the conclusion is that flaw density plays a more significant role than the average flaw size. The study shows that the rank orders of the mechanical material properties where consistent with the rank order of the experimentally determined particle rate of breakage. Materials that have a relatively low hardness show the largest particle rate of breakage. The degree of fracture tends to decrease for particles that have a smaller flaw density and hence behave more ductile. The study shows that pre-existing flaws have an impact on mechanical material properties and on particle fracture behaviour in a jet mill.

It is concluded that crystal's flaw size and density of flaws has an impact on the mechanical material properties and subsequently, on fracture behaviour of particles in a jet mill. Therefore, unit-operations like crystallization which has an impact on impurities and flaws in crystals, influences also the fracture behaviour of particles in a jet mill.

Acknowledgements

The contribution of W. Pries, Akzo Nobel who provided the sodium chloride of different sources is gratefully acknowledged. The nanoindentation samples were prepared by W. van der Zande, Philips Applied Technologies.

6.5 References

1. Timsina M.P., Martin G.P., Marriott C. Gander-ton D., Yianneskis M.,. 1994, Drug delivery to the respiratory tract using dry powder inhalers, *Int. Journal of Pharmaceutics* 101, 1-13
2. Chen Y., Ding Y., Papadopoulos D.G., Ghadiri M., 2004, Energy-based analysis of milling α-lactose monohydrate, *J. Pharm. Sci.* 93, 886-895
3. Nakach M., Authelin J., Chamayou A., Dodds J., 2002, Comparison of various milling technologies for grinding pharmaceutical powders, *10th European symposium on comminution*, Heidelberg, Germany
4. Zugner S., Marquardt K., Zimmerman I., 2006, Influence of nanomechanical crystal properties on the comminution process of particulate solids in spiral jet mills, *Eur. J. of Pharm. and Biopharm.* 62, 194-201
5. Peukert W., 2002, Material properties in fine grinding, *10th European symposium on comminution*, Heidelberg, Germany
6. Rumpf H., 1973, Physical aspects of comminution and new formulations of a law of comminution, *Powder Technol.* 7, 145-159

7. Heckel R.W., 1961, Density-pressure relationships in powder compaction. *Trans. Met. Soc. AIME* 221, 671-675
8. Heckel R.W., 1961b, An analysis of powder compaction phenomena, *Trans. Met. Soc. AIME* 221, 1001-1108
9. Roberts R.J., Rowe R.C., York P., 1987, The compaction of pharmaceutical and other model materials, *Chem. Eng. Sci.* 42, 903-911
10. Oliver W.C., Pharr G.M., 2002, *J. Mater. Res.* 7, 1564
11. Vegt O.M. de, Vromans H., Pries W., Voort Maarschalk K. van der, 2006, The effect of crystal imperfections on particle fracture behaviour, *Int. J. of Pharm.* 317, 47-53
12. Ward I.M., Hadley D.W., 1995, An introduction to the mechanical properties of solid polymers, John Wiley & Sons
13. Roberts R.J., Rowe R.C., 1987, The compaction of pharmaceutical and other model materials- a pragmatic approach, *Chem. Eng. Sci.* 42, 903-911
14. Ghadiri M., Zhang Z., 2002, Impact attrition of particulate solids. Part 1: A theoretical model of chipping, *Chem. Eng. Sci.* 57, 3659-3669
15. Tabor D., 1951, The hardness of metals, Clarendon Press. Oxford
16. Puttick K.E., Badrick A.S.T., 1987, The mechanical breakdown of sodium chloride crystals, *Chem. Eng. Sci.* 42, 855 – 868
17. Gahn A., Mersmann A., 1995, The brittleness of substances crystallized in industrial processes, *Powder Technol.* 85, 71-81
18. Vogel L., Peukert W., 2002, Characterisation of grinding-relevant particle properties by inverting a population balance model, *Part. Part. Syst. Charact.* 19, 149-157
19. Berthiaux H., Dodds J., 1999, Modelling fine grinding in a fluidized bed opposed jet mill Part 1: Batch grinding kinetics, *Powder Technol.* 106, 78-87

20. Weichert R., 1991, Theoretical prediction of energy consumption and particle size distribution in grinding and drilling of brittle materials, *Part. Part. Syst. Charact.* 8, 55-62
21. Inglis C.E., 1913, Stresses in a plate due to the presence of cracks and sharp corners, *Transactions of the Institution of Naval Architects* 55, 219-23
22. Wong R.H.C., Chau K.T., Tang C.A., Lin P., 2001, Analysis of crack coalescence in rock-like materials containing three flaws- Part 1: experimental approach, *Int. J. of Rock Mechanics & Minings Sciences* 38, 909 – 924
23. Horri H., Nemat-Hasser S., 1985, Compression induced microcrack growth in brittle solids: axial splitting and shear failure. *J. Geophys. Res.* 90, 3105-25
24. Horri H., Nemat-Hasser S., 1986, Brittle failure in compression: splitting, faulting and brittle-duction transition, *Phil. Trans Roy. Soc. London* A319, 497-510
25. Ashby M.F., Hallam S.D., 1986, The failure of brittle solids containing small cracks under compressive stress states., *Acta Metall.* 34, 497-510
26. Lankford J., Davidson L., 1979, The crack initiation threshold in ceramic materials subject to elastic/plastic indentation, *J. of Mat. Sci.* 14, 1662-1668
27. Evans A.G., Wilshaw T.R., 1976, Quasi static solid particle damage in brittle solids – 1. Observations, analysis and implications, *Acta Met*. 24, 939-955